Harmonical Characterization of a Microstrip Bend via the Finite Difference Time Domain Method

Noël Feix, Michèle Lalande, and Bernard Jecko, *Member, IEEE*

***Abstract*—A 90° Microstrip bend is characterized using a Time-Frequency method based on the Finite Difference Time Domain (FDTD) method. Time evolution of the currents generated by FDTD are Fourier transformed to lead to *S*-parameters and radiated powers characteristic of the microstrip bend. The method for calculating both radiation and surface wave losses is developed in this paper for microstrip structures. Then, the results of the 90° microstrip bend are compared with the results of the mitered microstrip bend.**

***Keywords*—Finite Difference Time Domain (FDTD) method; microstrip; bend; surface waves; space waves; radiation; miter.**

I. Introduction

INCREASE of integration density and of digital integrated circuits requires a rigorous analysis of propagation on microstrip interconnection lines. This analysis must give the degradation of line transported signals, for example due to the structure dispersion or to other line proximity [1]. In the same way, in microwave integrated circuits, rigorous microstrip structure models have to be elaborated in larger and larger bands.

To solve these problems, a lot of numerical resolution methods have been developed over the past few years, and particularly the transient ones. For digital circuits, a microstrip line analysis in the time-domain allows to have direct access to carried signals [2], [3]. On the other hand, for microwave circuit conception, the frequential characteristics of the structure are required. So, Fourier transforms follow the temporal analysis [4], [5].

With the object of precisely studying the microstrip behavior, the finite difference transient method has been chosen and adapted to a discontinuity characterization (right angle bend) [6]. On the one hand, the evolution of the scattering parameters as a function of frequency, related to the discontinuity, and on the other hand, surface waves (in the dielectric) and space waves (in the air) contribution to the total radiation are deduced from Fourier transforms of currents on the structure. So, a power balance can be established on every microstrip structure in a large frequency band.

This article includes several parts:

Manuscript received May 20, 1991; revised November 11, 1991.

The authors are with the Institut de Recherche en Communications Optiques et Microondes, Faculte des Sciences, Universite de Limoges 123 Avenue Albert-Thomas, F-87060 Limoges, Cedex, France.

IEEE Log Number 9106768.

The first part briefly presents the Finite Difference Method, and its application to the bend microstrip line characterization.

The second part describes the method of calculation of power, radiated by a microstrip structure, by using the stratified medium theory.

In the third part, we have compared theoretical and experimental results. The experimental results are obtained using a Wiltron 360 network analyzer. Then, we have studied the influence of a 45° miter.

II. Microstrip Structure Characterization by a Time Frequency Method Based on the Finite Difference Time-Domain Method

The transient simulation on microstrip lines is based on the FDTD. This method is described in [7].

It consists in a discretization of Maxwell's curl equations directly in time domain:

$$\overrightarrow{\text{curl}}\,\vec{E} = -\mu \frac{\partial \vec{H}}{\partial T} \tag{1}$$

$$\overrightarrow{\text{curl}}\,\vec{H} = \epsilon \frac{\partial \vec{E}}{\partial t} + \vec{J}. \tag{2}$$

To analyze an open structure, we have to divide not only the structure but also the surrounding space into meshes. To simulate the infinite space in a finite calculation domain, we surround the calculation volume with an "absorbing sheet" [8].

The analysis of a microstrip structure requires the definition of two media (Fig. 1) [8]:

1) medium with a relative permittivity ϵ_r (substrate) and,

2) medium representing the free space surrounding the structure.

The metal strip and the ground plane, supposed to be perfectly conductor and infinitely thin, are defined by setting the tangential component of the electric field to zero.

The line feed is simulated by a vertical electric field component in a plane located between the strip and the ground plane (excitation plane). The time gaussian shaped excitation allows a harmonic characterization on a large frequency band. The FDTD algorithm provides $\vec{E}$ and $\vec{H}$ field components in the total calculation volume and at each temporal sampling step. The temporal current evo-

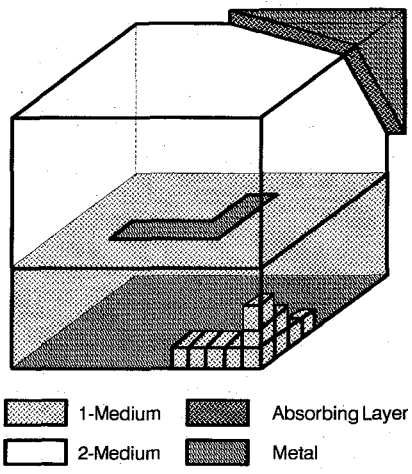

Fig. 1. Definition of a calculation domain.

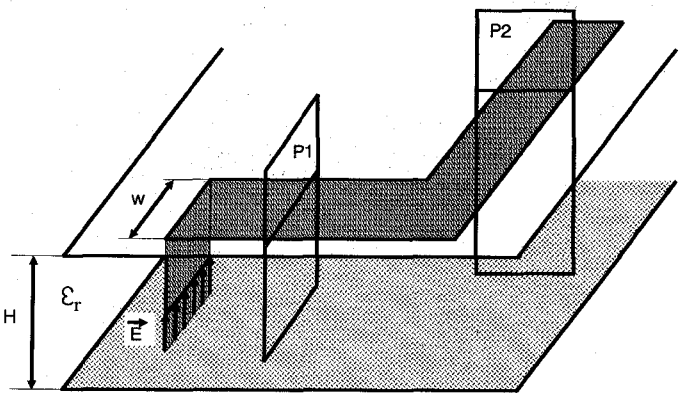

Fig. 2. Microstrip feed and reference planes.

lution on the line is deduced from $\vec{H}$ field circulation around the conductor strip.

Harmonic discontinuity characterization follows this transient analysis and is divided into two stages:

Scattering Parameter Calculation: Two reference planes P_1 and P_2 are chosen as shown in Fig. 2. Scattering parameters are deduced from incident, reflected by the discontinuity (calculated in P_1) and transmitted currents (calculated in P_2) as follows:

$$S_{11}(f) = \frac{\mathcal{F}(I_{\text{reflected}}(t))}{\mathcal{F}(I_{\text{incident}}(t))}$$

$$S_{21}(f) = \frac{\mathcal{F}(I_{\text{transmitted}}(t))}{\mathcal{F}(I_{\text{incident}}(t))}. \tag{3}$$

Radiated Power Determination—Power Balance: The powers lost by radiation between the reference planes are now calculated. Comparison between P_1 incident power, P_1 reflected power, P_2 transmitted power and the radiated discontinuity powers permit to establish a power balance.

The radiated power calculation principle is described in the following chapter.

III. Radiated Power by a Microstrip Line Section—Power Balance

The FDTD algorithm provides I_x (and I_z) current in every metallic strip point. An electric dipole (Hertz dipole) is associated at each component I_x with moment $I_x \Delta x$ (and $I_z \Delta z$) located at the air-dielectric interface.

The first calculation stage consists in giving the expression of the $\vec{E}$ and $\vec{H}$ fields radiated by only one electric dipole in every space point. The field radiated by this dipole is expressed in term of Hertzian potentials [9]:

$$\vec{H} = \frac{jk_i^2}{\omega\mu_i} \vec{\nabla} \Lambda \vec{\Pi}_i \tag{4}$$

$$\vec{E} = \vec{\nabla}(\vec{\nabla} \cdot \vec{\Pi}_i) + k_i^2 \vec{\Pi}_i \tag{5}$$

where

$k_i = \omega \sqrt{\mu_i \epsilon_i}$
ϵ_i: permittivity of the medium
μ_i: magnetic permeability of the medium
Π_i: Hertzian potential
$i = 0$, air
$i = 1$, dielectric

The application of the Steepest Descent Path (SDP) method allows to obtain the far field components [10]. The far field results from the superposition of two terms [11]:

The first term is associated to the spherical space waves radiation in the air, its amplitude decreases with $1/r$ (Fig. 3).

The second one is associated to the cylindrical surface waves, it originates in singularities of Hertzian potentials. Its amplitude decreases with $1/\sqrt{\rho}$ (Fig. 3).

Space Spherical Wave Radiated Power Created by the Electric Dipole: The far radiated electric field created by an elementary dipole with $I_x \Delta x$ are given in [12].

Then, the Hertzian dipole radiated power is obtained by a power surface density integration on r radius semisphere (Fig. 4):

$$Pr = \int_0^{2\pi} \int_0^{\pi/2} \frac{1}{2Z_0} \{ |E_\theta(r, \theta, \phi)|^2 + |E_\phi(r, \theta, \phi)|^2 \} r^2 \sin\theta \, d\theta \, d\phi \tag{6}$$

with: $Z_0 = \sqrt{\mu_0/\epsilon_0}$, characteristic impedance in the vacuum.

Cylindrical Surface Wave Radiated Power Created by the Electric Dipole: Surface waves are constituted by different propagation modes [13]: a fundamental mode with a cutoff frequency equal to zero, upper-modes with cutoff frequencies as follows:

$$fc = \frac{nc}{4H\sqrt{\epsilon_r - 1}} \tag{7}$$

$n = 1, 3, 5, \cdots$ TE_n mode
$n = 0, 2, 4, \cdots$ TM_n mode
c: light velocity
H: substrate height
ϵ_r: relative permittivity

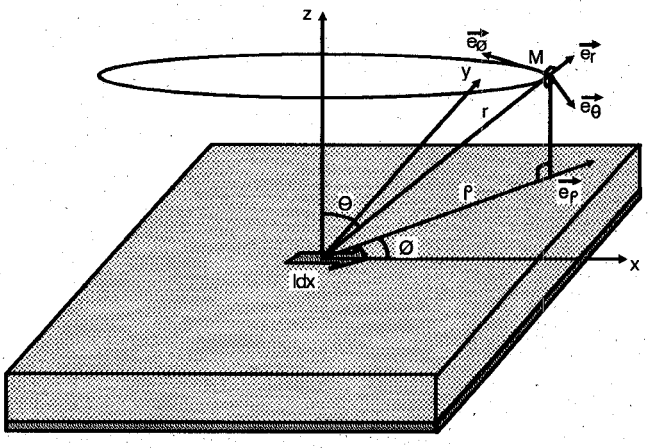

Fig. 3. Hertz dipole radiation.

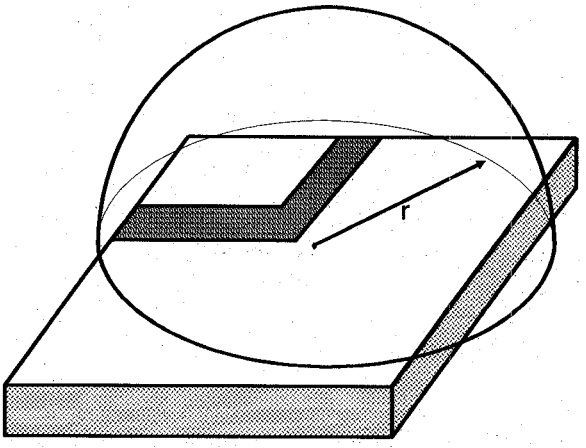

Fig. 4. Power surface density integration on r radius semi-sphere.

We will suppose that the cutoff frequency (TE_1) is out of the considered frequency band.

In that case, the Hertzian potential has only one component in Z direction. The radiated far fields are given in [14].

The TM_0 surface wave spreads with no attenuation in a air-dielectric interface parallel direction, whereas it decreases in perpendicular direction. The power carried by this wave is obtained by power surface density integration on a semi-cylinder with ρ radius and infinite height. (Fig. 5).

$$P_{TM_0} = -\frac{1}{2}\int_0^{+\infty}\int_0^{2\pi} E_{zTM_0}(\rho, \phi, z) \cdot H^*_{\phi TM_0}(\rho, \phi, z)\rho \, d\phi \, dz. \quad (8)$$

Generalization to a Radiating Surface—Power Balance: The radiating surface is considered as the association of M dipoles with moment $I_x \, \Delta x$, directed along $\vec{e}_x$, and of $N\cdot$ dipoles with moment $I_y \, \Delta y$, turned following (Fig. 6).

Then, network theory gives radiated fields produced by any form surface [11].

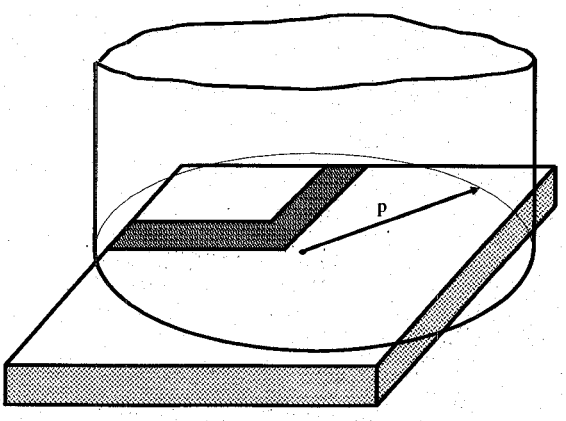

Fig. 5. Power surface density integration on an infinite height semi-cylinder.

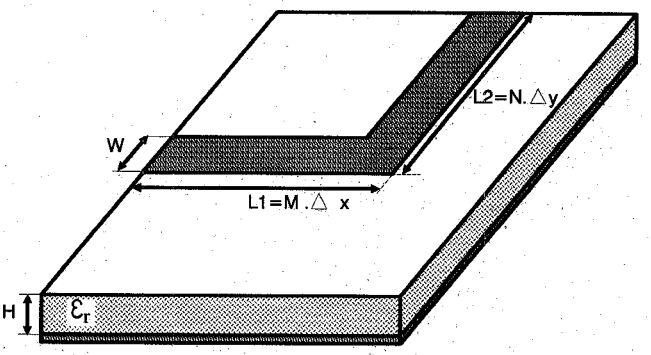

Fig. 6. Microstrip line characteristics.

Spherical coordinates (for space waves):

$$E_\alpha(r, \theta, \phi) = \sum_{i=1}^{M} E_{\alpha i}(r, \theta, \phi) \exp(jk_0 \vec{e}_r \vec{\rho}_i) + \sum_{j=1}^{N} E_{\alpha j}\left(r, \theta, \phi - \frac{\Pi}{2}\right) \exp(jk_0 \vec{e}_r \vec{\rho}_j)$$

with: $\alpha = \theta$ or ϕ (9)

Cylindrical coordinates (for surface waves):

$$E_\alpha(\rho, \phi, z) = \sum_{i=1}^{M} E_{\alpha i}(\rho, \phi, z) \exp(\lambda_s \vec{e}_\rho) + \sum_{j=1}^{N} E_{\alpha j}\left(\rho, \phi - \frac{\Pi}{2}, z\right) \exp(\lambda_s \vec{e}_\rho)$$

with: $\alpha = \phi$ or z

λ_s: pole of the Hertzian Potential (10)

Then, it is possible to establish a power balance by comparing the following values:

Incident power,
Reflected power (deducted from S_{11})
Transmitted power (deducted from S_{21})
Spherical wave radiated power
Cylindrical wave radiated power.

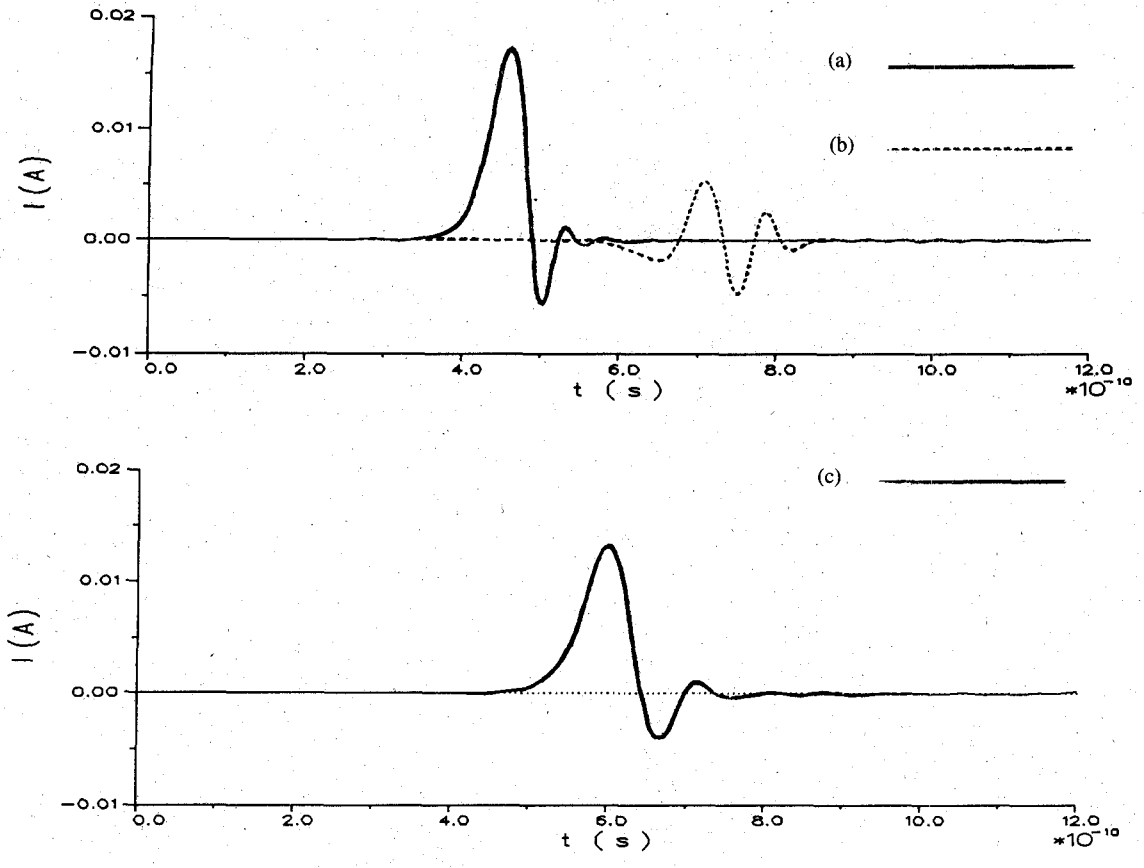

Fig. 7. Current time evolution. (a) Incident current (P_1). (b) Reflected current (P_1). (c) Transmitted current (P_2).

The incident power is obtained by a Poynting's vector integration on the P_1 incident plane. We neglect here the dissipation power in both the metal plates and the dielectric substrate.

IV. Theoretical and Experimental Results

The studied microstrip has the following characteristics (Fig. 6), $W = 3$ mm, $\epsilon_r = 4.5$ (epoxy substrate), $H = 1.6$ mm, $L_1 = 19.8$ mm and $L_2 = 9$ mm.

We give meshes size and number used in finite difference algorithm in the three space directions the following values: $\Delta_x = 0.6$ mm, $N_x = 292$, $\Delta_y = 0.6$ mm, $N_y = 152$, $\Delta_z = 0.4$ mm and $N_z = 28$.

The total time steps is 1000.

The Gaussian excitation has a 37.5 ps half height width and a 27 ps rise time (10%–90%). So, its spectrum covers the frequency band in which we want to characterize the structure: 0–14 Ghz.

The incident, reflected and transmitted (in P_1 and P_2) currents are shown in Fig. 7.

A. Frequency Characterization of the Microstrip Bend

In our study, only the TM_o surface wave mode is excited; the TE_1 mode cutoff frequency (25 GHz) being superior to the maximum frequency of the band in which the discontinuity is characterized.

The S parameters of the discontinuity, deduced from the transient current Fourier's transforms are shown in Figs. 8 and 9. On these figures, measurement results from a WILTRON 360 network analyzer are given. For the experimentation, the distance between the connectors and the discontinuity is identical to the distance between the reference planes and the discontinuity in the theory.

The S_{21} frequency evolution shows that the bent line performs as a low-pass filter which cut-off frequency is about 10 GHz (Fig. 8).

The line characteristic impedance is the reference impedance for theoretical S-parameters. This impedance is equal to 50 Ω at low-frequencies, and differs from this value when the frequency increases, because of the dispersion. 50 Ω is the reference impedance for measured S-parameters, and because of the difference at high frequencies between Z_c and 50 Ω, resonances can be noticed.

In fact, resonant frequencies that appear experimentally, are rather due to the connector-strip junction imperfection than to the mismatching. These resonances are dependent either on the distance between the two reference planes (about 3.5 GHz multiples) (Fig. 8), or on the distance between the alimentation access and the discontinuity (about 5 GHz multiples) (Fig. 9).

However, in this example, theoretical results are validated by experimentation.

The difference between $\|S_{11}\|^2 + \|S_{21}\|^2$ and unity (Fig. 10) shows that an important part of the power is lost

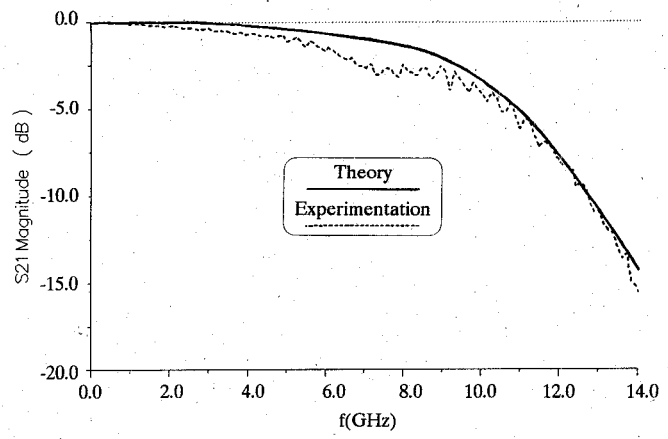

Fig. 8. Transmission coefficient magnitude S_{21}. Comparison between theoretical and experimental results.

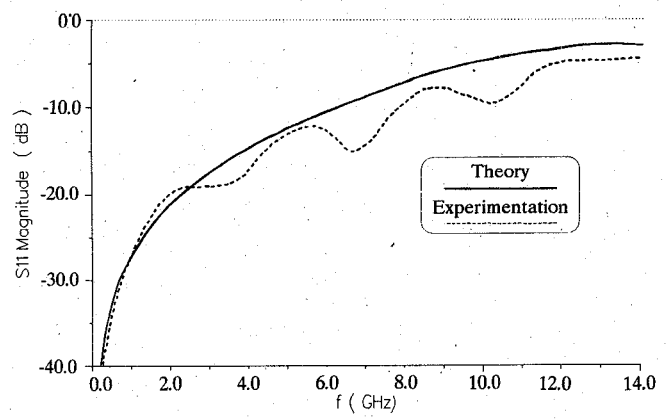

Fig. 9. Reflection coefficient magnitude S_{11}. Comparison between theoretical and experimental results.

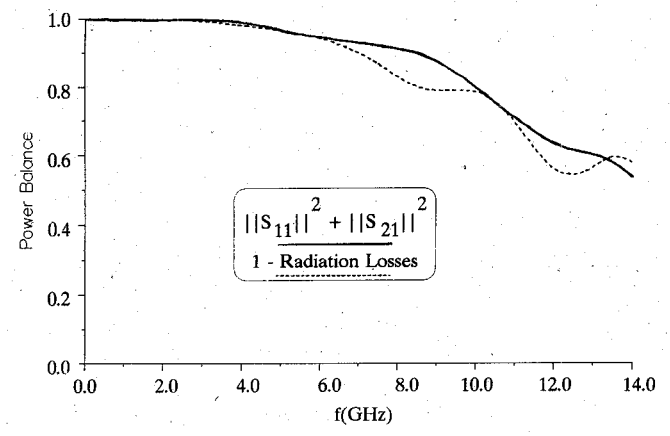

Fig. 10. Power balance.

at the considered high frequencies. Space and surface wave radiated power is calculated following the method described in Section II.

Oscillations appear on the space and surface wave radiated powers (Fig. 11). These oscillations are due to the truncation of the current spatial distribution on the structure, especially those that are located between the reference plane and the discontinuity. Resonant frequencies are depending on the L_1 length.

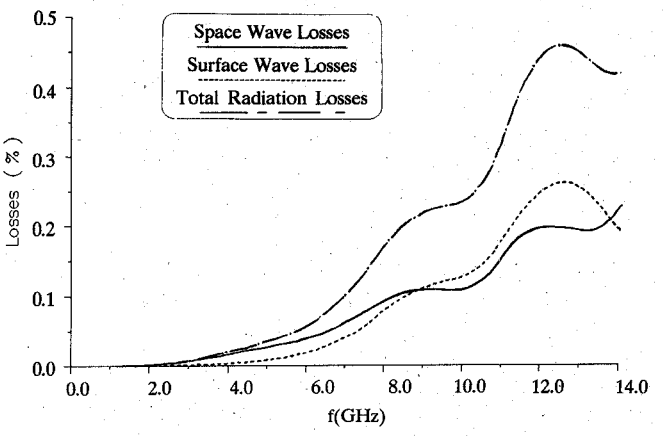

Fig. 11. Radiation losses.

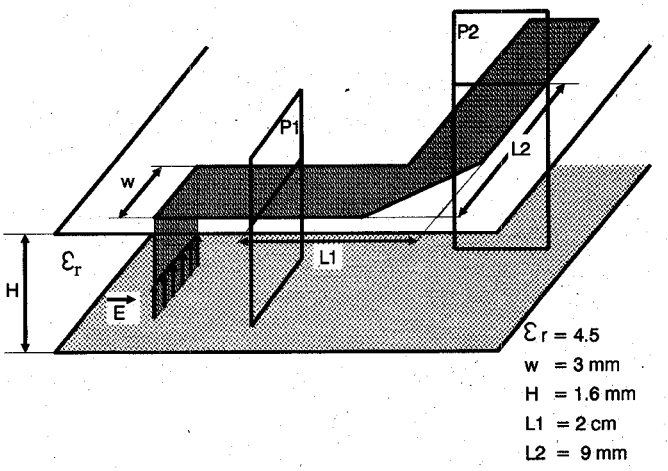

Fig. 12. Mitered microstrip bend.

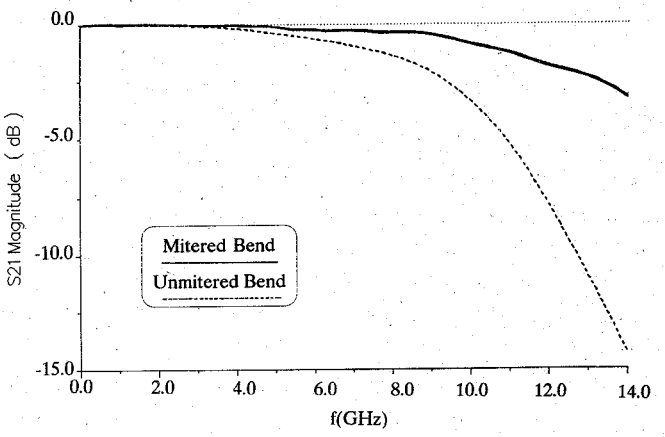

Fig. 13. Transmission coefficient magnitude S_{21}. Comparison between mitered and unmitered bend.

However, the curves representing the evolution as a function of frequency (Fig. 10):

$$-\|S_{11}\|^2 + \|S_{21}\|^2 \quad \text{and}$$

$$-1 - \text{radiation losses}$$

are very close.

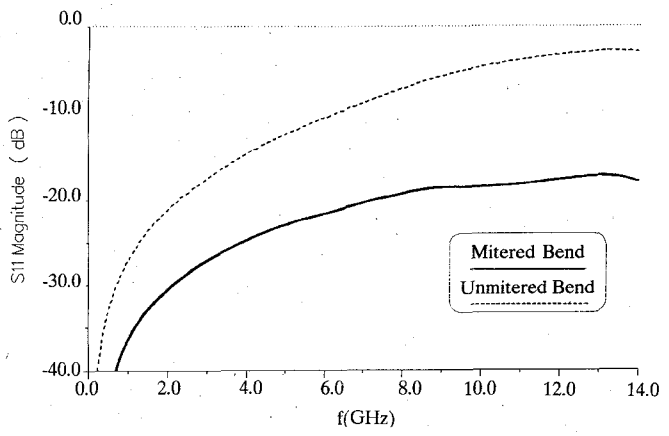

Fig. 14. Reflection coefficient magnitude S_{11}. Comparison between mitered and unmitered bend.

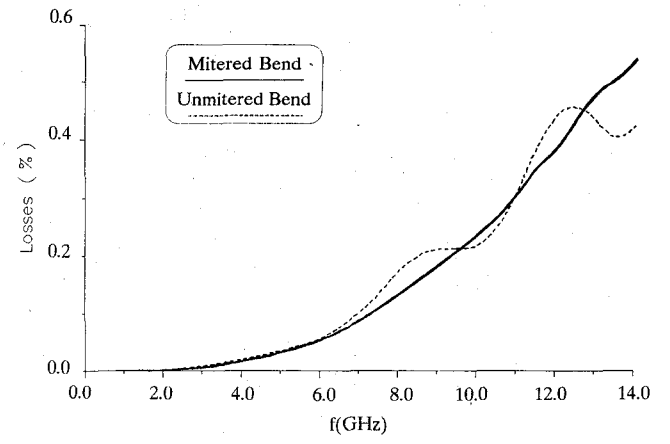

Fig. 15. Radiation losses. Comparison between mitered and unmitered bend.

B. Miter Influence on the Frequency Characteristics

Fig. 12 shows the 90° microstrip bend with a 45° miter. The frequency characterization of the Mitered bend is obtained in the same way as that for the unmitered bend.

Figs. 13 and 14 show the scattering parameters magnitude for the microstrip bend with and without miter. We can see that the reflection coefficient is higher and the transmission coefficient is smaller when the bend is unmitered. The difference can attain 15 dB for the reflection parameter and 11 dB for the transmission parameter. However, the radiated losses are approximately identical in the two cases (Fig. 15).

V. Conclusion

The FDTD method is used to simulate and characterize a microstrip discontinuity (a 90° bend). Then, harmonical characterization is elaborated on a frequency band directly linked to the chosen excitation form, and is realized from the scattering parameters, the space wave and surface wave radiated power. A good agreement between measured and calculated S-parameters for a right angle microstrip bend have validated theoretical method. The method allows to dissociate the space and surface wave contribution at the total structure radiation and to evaluate a power balance.

A comparative study between a bend with and without miter has shown that even if the bend induced less reflection, the total radiated power has approximately the same value.

References

[1] J. Chilo, "Modélisation et analyse temporelle d'un bus d'interconnexion en technologie GaAs," *Annales des Télécommunications*, 40, no. 3-4, pp. 135-144, 1985.

[2] T. Leung and C. A. Balanis, "Attenuation distorsion of transient signals in microstrip," *IEEE Trans. Electromagn. Compat.*, vol. 36, no. 4, pp. 765-769, Apr. 1988.

[3] X. Zhang, J. Fang, K. K. Mei, and Y. Liu, "Calculations of the dispersive characteristics of microstrips by the time-domain finite difference method," *IEEE Trans. Microwave Theory Tech.*, vol. 36, no. 2, pp. 263-267, Feb. 1988.

[4] X. Zhang and K. K. Mei, "Time-domain finite difference approach to the calculation of the frequency-dependent characteristics of microstrip discontinuities," *IEEE Trans. Microwave Theory Tech.*, vol. 36, no. 12, pp. 1775-1787, Dec. 1988.

[5] D. M. Sheen, S. M. Ali, M. D. Abouzarha, and J. A. Kong, "Application of the three-dimensional finite-difference time-domain method to the analysis of planar microstrip circuits," *IEEE Trans. Microwave Theory Tech.*, vol. 38, no. 7, pp. 849-857, July 1990.

[6] J. Moore and H. Ling, "Characterization of a 90° microstrip bend with arbitrary miter via the time-domain finite difference method," *IEEE Trans. Microwave Theory Tech.*, vol. 38, no. 4, pp. 405-410, Apr. 1990.

[7] K. S. Yee, "Numerical solution of initial boundary value problems involving Maxwell's equations in isotropic media," *IEEE Trans. Antennas Propagat.*, vol. 14, no. 3, pp. 302-307, May 1966.

[8] A. Reineix, "Analysis of Microstrip Patch Antennas Using Finite-Difference Time Domain Method," *IEEE Trans. Antennas Propagat.*, vol. 37, no. 11, pp. 1361-1369, Nov. 1989.

[9] N. G. Alexopoulos and D. R. Jackson, "Fundamental superstrate (cover) effects on printed circuit antennas," *IEEE Trans. Antennas Propagat.*, vol. AP-32, pp. 807-816, Aug. 1984.

[10] J. R. Mosig and F. E. Gardiol, "Rayonnement d'une antenne microruban de forme arbitraire," *Annales des Télécommunications*, vol. 40, no. 3-4, pp. 181-189, 1985.

[11] N. G. Alexopoulos, D. R. Jackson, and P. B. Katehi, "Criteria for nearly omnidirectional radiation patterns for printed antennas," *IEEE Trans. Antennas Propagat.*, vol. AP-33, pp. 195-205, Feb. 1985.

[12] J. Herault, R. Moini, and B. Jecko, "Analyse de microantennes par une méthode temporelle," *Annales des Télécommunications*, vol. 42, no. 9-10, pp. 578-585, 1987.

[13] T. Itoh, *Numerical Techniques for Microwave and Millimeter-Wave Passive Structures*. New York: Wiley-Interscience, 1989.

[14] J. Herault, R. Moini, A. Reineix, and B. Jecko, "A new approach to microstrip antennas using a mixed analysis: Transient-frequency," *IEEE Trans. Antennas Propagat.*, vol. 38, no. 8, pp. 1166-1175, Aug. 1990.

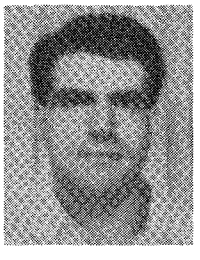

Noël Feix, was born in Brive, France, in 1963. He received the Diplome d'Etudes Approfondies in Electronic. He is presently studying for obtaining the Doctorat in Electronic from the University of Limoges, Limoges, France, in the Laboratory of Electectromagnetism of the Institut de Recherches en Communications Optiques et Microondes (IRCOM). He is now engaged in research on propagation problems on microstrip lines.

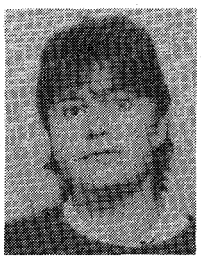

Michèle Lalande, was born in Noth, France, in 1962. She received the Doctorat in Electronic from the University of Limoges, Limoges, France, in 1986.

Presently, she is a Lecturer at the University Institute of Technology of Limoges (Department Electric Engineering and Industrial Computer Science, Brive, France) and is member of the Electromagnetic Team of the Institut de Recherches en Communications Optiques et Microondes (IRCOM). She is currently engaged in research on propagation problems on microstrip lines.

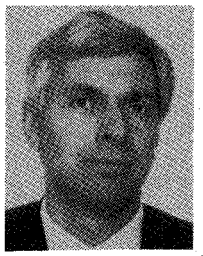

Bernard Jecko, was born in Trelissac, France, in 1944. He received the Doctorat Third Cycle and the Doctorat es Sciences degrees from the University of Limoges, Limoges, France, in 1971 and 1979, respectively.

He is currently a Professor at the University of Limoges and leads the Electromagnetic Team of the Institut de Recherches en Communications Optiques et Microondes (IRCOM). His research interest is in the area of electromagnetic wave diffraction theory, particularly in the time domain.